Journal of Nanophotonics

Nanophotonics.SPIEDigitalLibrary.org

Impact of temperature on the linewidth enhancement factor of chirped InAs/InP broadband quantum-dash lasers around 1610 nm

Mohammed Zahed Mustafa Khan

Mohammed Zahed Mustafa Khan, "Impact of temperature on the linewidth enhancement factor of chirped InAs/InP broadband quantum-dash lasers around 1610 nm," *J. Nanophoton.* **13**(2), 026001 (2019), doi: 10.1117/1.JNP.13.026001.

Impact of temperature on the linewidth enhancement factor of chirped InAs/InP broadband quantum-dash lasers around 1610 nm

Mohammed Zahed Mustafa Khan*
King Fahd University of Petroleum and Minerals, Optoelectronics Research Laboratory, Electrical Engineering Department, Dhahran, Saudi Arabia

Abstract. We report on the effect of temperature on the differential gain, differential refractive index, and linewidth enhancement factor (α-factor) of ∼1610-nm chirped barrier thickness multi-stack InAs quantum-dash (Qdash)-in-a-well laser diodes with an extended active region inhomogeneity. By employing Hakki–Paoli method, the performance is found to be comparable at a lower temperature region (16°C to 25°C), exhibiting higher differential gain and lower α-factor values of $\sim 0.7 \pm 0.1\ \mathrm{cm}^{-1}\,\mathrm{mA}^{-1}$ and $\sim 2.6 \pm 1.0$, respectively, at gain maximum. At higher temperatures of 25°C to 35°C, the performance degrades mainly due to drop of the differential gain at a rate of $\sim 0.03\ \mathrm{cm}^{-1}\,\mathrm{mA}^{-1}\,{}^{\circ}\mathrm{C}^{-1}$ and α-factor values reaching $\sim 4.7 \pm 2.0$ at 40°C. The room temperature (20°C) measured values are in good agreement with the literature, and we qualitatively explain the temperature influence on these results from the highly inhomogeneous Qdash system viewpoint. This study will assist in further optimization of these nanostructure-based high active region gain laser devices that are promising candidates in L-band optical communications, capable of providing low-frequency chirp and high-performance operation. © *2019 Society of Photo-Optical Instrumentation Engineers (SPIE)* [DOI: 10.1117/1.JNP.13.026001]

Keywords: InAs/InP quantum-dash lasers; linewidth enhancement factor; differential gain; semiconductor broadband lasers.

Paper 19022 received Feb. 6, 2019; accepted for publication Mar. 29, 2019; published online Apr. 16, 2019.

1 Introduction

There has been growing interest in employing InAs/InP quantum-dash (Qdash) nanostructure-based active region for lasers and amplifiers and their potential applications in optical access networks. Thanks to the broad tunability of Qdash emission spanning S-, C- and L-band wavelength region[1–3] hence offering the possibility to realize III–V semiconductor-based devices in the extended wavelength bands (L-band), which is under consideration as one of the potential solutions to curb the data traffic in future optical access networks.[3] Several significant characteristics of InAs/InP Qdash lasers and amplifiers have been demonstrated, for instance, broadband and multiwavelength emission,[4,5] subpicosecond pulse generation,[6] reduced timing jitter,[7] fast gain recovery,[8] etc. Hence, a thorough understanding of the InAs/InP Qdashes as gain material is essential, even at high temperatures, to further optimize the device structures and their performance. Fundamental parameters such as gain, differential gain ($\mathrm{d}g/\mathrm{d}I$), differential refractive index ($\mathrm{d}n/\mathrm{d}I$), and α-factor are such vital indicators that determine the dynamic performance of lasers, such as linewidth, frequency chirp, feedback sensitivity, nonlinear dynamics including under optical feedback, filamentation, four-wave mixing, etc.[9] In literature, α-factor of InAs/InP Qdash laser has been evaluated by Hakki–Paoli (H-P),[10] frequency-modulation/amplitude-modulation (FM/AM),[11] and injection locking (IL) methods.[9] In the following, we briefly review these works; $\mathrm{d}g/\mathrm{d}I$ and below threshold α-factor of $0.07\ \mathrm{cm}^{-1}\,\mathrm{mA}^{-1}$ and ∼2.0, respectively, have been reported on fixed barrier thickness as-grown InAs/AlGaInAs/InP Qdash laser diodes at ∼1610 nm, and the effect of postgrowth intermixing on the device dynamics was also evaluated.[10] In this intermixed case, $\mathrm{d}g/\mathrm{d}I$ and α-factor

*Address all correspondence to Mohammed Zahed Mustafa Khan, E-mail: zahedmk@kfupm.edu.sa

1934-2608/2019/$25.00 © 2019 SPIE

in the range of 0.05 to 0.1 cm^{-1} mA^{-1} and ~2.1 to 3.6, respectively, are reported, thus retaining the active region material quality postintermixing.[10] In other works, a below threshold α-factor of ~3.3 was measured at ~1606-nm gain peak by Ukhanov et al.[12] from InAs/AlGaInAs/InP Qdash laser. Mi and Bhattacharya[13] demonstrated significant reduction in the α-factor reaching ~0 to 2.0 at ~1650 nm via p-doping the active region and eventually to ~0 to 0.7 by an additional tunnel injection active region, on Qdash lasers at ~1620 nm. On a different InAs/InGaAsP/InP Qdash laser active region, Lelarge et al.[14] reported an α-factor of ~5.0 to 7.0 at ~1550 nm. In all these investigations, the well-recognized H-P technique has been employed for the measurement and calculation of the laser dynamic characteristics.

Recently, FM/AM and IL techniques are gaining attention owing to their ability to depict the α-factor above the threshold, which is not possible by H-P method. By employing the former method, Wang et al.[9] reported below threshold α-factor values of ~2.5 to 3.0 on 1550-nm InAs/InP Qdash laser devices, and Lester et al.[15] and Hein et al.[11] utilized the latter IL technique to investigate the dynamic characteristics of InAs/InP Qdash lasers in C- and near L-bands. While the former work reported a below threshold α-factor of ~2.0 to 3.0 at ~1550 nm and ~5.0 at ~1580 nm without optical feedback, and a significantly reduced value of ~0 to 2.0 in the feedback configuration,[15] an above threshold α-factor of ~2.5 to 4.0 was reported in the latter work on the Qdash lasers. Lately, IL and H-P techniques are also employed on InAs/InP quantum-dot laser exhibiting <1.0 below threshold and ~1.4 to 1.6 above threshold α-factor near peak gain at ~1520 nm,[16] and below threshold α-factor of ~0 to 2.0 around ~1560 nm from tunnel injection InAs/InP quantum-dot lasers.[17] In general, these reported works on Qdash lasers employed conventional multistack active region with fixed barrier thickness (unchirped devices). However, the effect of intentionally extended inhomogeneous broadening of Qdash laser (chirped devices) on α-factor and its performance at high operating temperature have not been investigated yet, to the author's knowledge.

In this work, we report, for the first time to our knowledge, the measured temperature-dependent differential gain, differential refractive index change, and α-factor of multistack chirped barrier thickness InAs/AlGaInAs/InP Qdash-in-a-well broadband laser with central wavelength at ~1610 nm. These below threshold dynamic characteristics parameters are obtained by H-P method and compared with the literature, showing good agreement, exhibiting α-factor of $\sim 2.5 \pm 1.0$ and a better differential gain of $\sim 0.65 \pm 0.1$ cm^{-1} mA^{-1} at gain maximum and at temperatures ≤25°C. However, the performance degraded with increasing temperature and the corresponding values reached $\sim 4.0 \pm 1.5$ $(\sim 4.6 \pm 2.0)$ and $\sim 0.26 \pm 0.14$ $(\sim 0.23 \pm 0.1)$ cm^{-1} mA^{-1} at 35°C (40°C), owing chiefly to the drop in dg/dI. This investigation is crucial for further optimization of the InAs/InP Qdash-based active region laser, which is a promising source in L- and C-band next-generation optical access networks, with recent potential demonstrations.[18]

2 Device Structure and Experimental Method

The InAs Qdashes are grown in an asymmetric 7.6 nm compressively strained AlGaInAs quantum-well (Qwell) and then covered with a variable thickness AlGaInAs barrier layer. Four such stacks were grown with barrier thicknesses of 20, 15, 10, and 10 nm, and later sandwiched between 200-nm lattice matched AlGaInAs separate confinement heterostructure layer (SCH) for efficient carrier confinement. This intrinsic active region is later enclosed between p- and n-type InAlAs top and bottom cladding layers, respectively, and on 001 n-type InP substrate, as shown in the schematic diagram of Fig. 1(a). Ridge waveguide lasers of 3- and 4-μm ridge width and 700- to 800-μm cavity length are fabricated from the aforementioned epitaxial structure with as-cleaved facets utilizing a standard laser fabrication process. More details of the device structure, fabrication, and characterization can be found elsewhere.[2,3] To minimize the interference of junction heating on the measurement results due to carrier surge, we employed pulsed current operation with 0.5-μs pulse width and 0.2% duty cycle to drive the laser below the threshold. The laser diode is mounted in a p-side up configuration and placed on a heatsink with a temperature controller, to monitor as well as alter the temperature operation with an accuracy of ±1°C. Then, the optical power is coupled into an in-house made singlemode lensed fiber (SMF), as illustrated

(a)

MATERIAL	LAYER	THICKNESS
InGaAs	Contact	250 nm
InAlAs	*p*-type	1900 nm
InGaAlAs	SCH	200 nm
InGaAlAs	Barrier	10 nm
InAs/InGaAlAs	Qdash-in-Qwell	5 ML/7.6 nm
InGaAlAs	Barrier	10 nm
InAs/InGaAlAs	Qdash-in-Qwell	5 ML/7.6 nm
InGaAlAs	Barrier	15 nm
InAs/InGaAlAs	Qdash-in-Qwell	5 ML/7.6 nm
InGaAlAs	Barrier	20 nm
InAs/InGaAlAs	Qdash-in-Qwell	5 ML/7.6 nm
InGaAlAs	Barrier	25 nm
InGaAlAs	SCH	200 nm
InAlAs	*n*-type	1000 nm
InP	*n*-type	~100 μm

(b) (c)

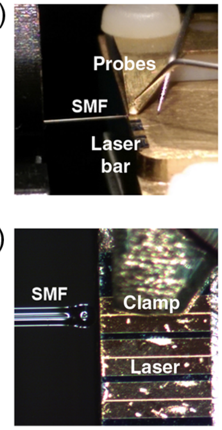

Fig. 1 (a) Schematic of the chirped barrier thickness InAs/InP Qdash laser device structure. (b) The unmounted and unbonded 800-μm cavity length fabricated laser diode bar placed in *p*-side up configuration with one device being probed. (c) Zoomed view of the probed bare Qdash laser diode whose optical power is coupled into a SMF for gain and F-P mode shift measurements. ML: Monolayer.

in Figs. 1(b) and 1(c), and the amplified spontaneous emission (ASE) spectra are taken on an optical spectrum analyzer with 0.05-nm resolution. The net modal gain is extracted at various current values below the threshold by measuring the peak-to-valley ratio of each longitudinal Fabry–Perot (F-P) mode of the ASE, whereas the refractive index change is obtained by measuring the respective mode wavelength shift with current injection. The α-factor is then calculated from the $\mathrm{d}g/\mathrm{d}I$ and $\mathrm{d}n/\mathrm{d}I$ values.[10,13,14] We have tested different devices, extracted these parameters, and then plotted their average values along with the corresponding variations, which is observed across the devices as well as different combinations of two currents below the threshold, for the analysis.

3 Results and Discussion

Figure 2(a) compares the below threshold net modal gain spectra of the chirped barrier thickness InAs/InP Qdash laser diode at various heatsink temperatures from 16°C to 40°C, obtained under normalized injection current I/I_{th} ratio of ~0.88. A gain bandwidth of more than 50 nm is apparent from Fig. 2(a) at all operating temperatures, an effect of intentionally dispersing the dash sizes and hence their transition energy states via altering the barrier thicknesses of the multistack active region. Moreover, from the summarized results of Fig. 2(b), a peak gain $g_{\max}$ of $\sim 3.9 \pm 0.2\ \mathrm{cm}^{-1}$ is measured at $\sim 0.88 I_{\mathrm{th}}$ and at temperatures 16°C to 35°C with an observation of ~8-nm redshift in the peak wavelength λ_g (i.e., from ~1615 to ~1623 nm). While for 40°C, the current injection is restricted to $\sim 0.78 I_{\mathrm{th}}$ exhibiting $g_{\max}$ of $\sim -0.4\ \mathrm{cm}^{-1}$ at λ_g of ~1630 nm. It is to be noted that we selected smaller normalized bias currents at high temperatures in order to minimize any arising optical nonlinearities and lateral cavity resonances from the high gain and dispersive dash size system[1,8,14] that might alter the F-P mode wavelength spacing. In fact, with increasing temperature and current injection (i.e., $> \sim 0.88 I_{\mathrm{th}}$ at 35°C and $> \sim 0.78 I_{\mathrm{th}}$ at 40°C), we observed appearance of additional F-P modes in the ASE spectra possibly due to lateral cavity resonance, thus masking the actual F-P modes wavelength spacing and power, hence rendering the data analysis difficult. The observed redshift of ~8 nm in λ_g with increasing temperature and constant electrical pumping is attributed to the transition energy shrinkage of the Qdash active region. In this case, the radiative recombination arising from the dominating intermediate average height dash ensemble now exhibits relatively smaller transition energy levels (longer wavelength emission) due to elevated junction temperature. However, the peak gain at 40°C, which is significantly lower than other temperatures and observed at even longer λ_g of ~1630 nm [see Fig. 2(a)], is ascribed to the effect of different pumping conditions, and hence a direct comparison with other temperatures is difficult. Nevertheless, in general, the gain

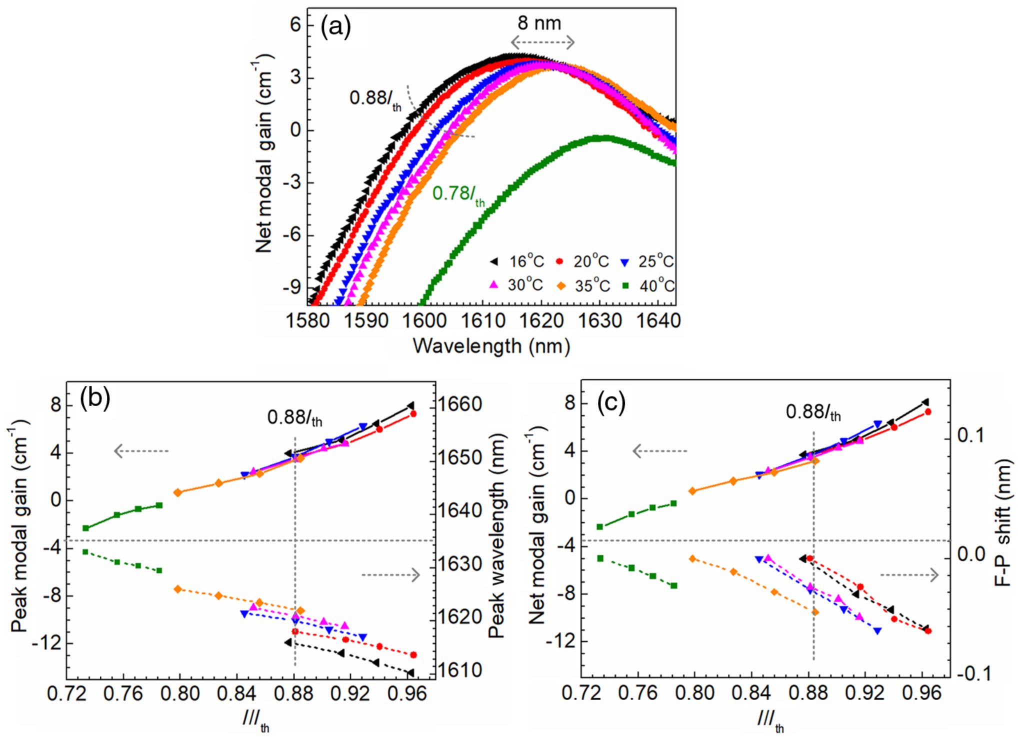

Fig. 2 Measured (a) below threshold gain spectra of InAs/InP Qdash laser diode at different operating temperatures, (b) net modal gain maximum $g_{\max}$ and the respective wavelength λ_g and (c) net modal gain and respective F-P mode wavelength shift, taken near $g_{\max}$, versus the below threshold injection current and obtained at various operating temperatures. All the gain spectra in (a) are obtained at $\sim 0.88 I_{th}$ except the one at 40°C, which is taken at $\sim 0.78 I_{th}$. The color markers of (b) and (c) follow the legend of (a).

spectra are found to be more symmetric with increasing temperature, suggesting a uniform and wider distribution of carriers among the inhomogeneous dash ensembles, assisted by elevated temperatures.

Next, in Fig. 2(b), we plot the λ_g shift and the corresponding $g_{\max}$ as a function of various normalized bias current below the threshold and at all heatsink temperatures. A rise in $g_{\max}$ and a blueshift in λ_g with increasing current injection are apparent at all temperature. This is a legacy of band filling effect, i.e., small average height dash ensemble with larger transition energies ($\sim 1.24/\lambda_g$) are getting occupied and consequently dominating the ASE and hence gain spectra. Moreover, the observation of redshift of λ_g with temperature rise is due to the temperature-dependent Qdash transition energy shrinkage as discussed above. On the other hand, referring to Fig. 2(c) that plots a particular F-P mode wavelength shift near λ_g and the corresponding net modal gain with increasing bias at all temperatures, a blueshift of mode wavelength at a constant temperature is evident. Since the carrier density in the active region determines the effective refractive index of the medium below the threshold, any increase in the injection current decreases the refractive index of the active region and thus blueshifts the F-P mode.[9,10,12] It is noteworthy to mention that an almost linear dependence of the net modal gain and F-P shift versus various injection current is also noticeable at all temperatures. While an approximately constant net modal gain slope is observed at all temperature, the slope of F-P mode blueshift shrinks with rising temperature and is reasonably noticeable at ≥35°C. We ascribe this latter observation, in part, again to the increasing carrier density (or injection current) with the rising temperature that decreases the refractive index of the active region and hence reducing the F-P blueshift phenomenon. In addition, this observation is also attributed partially to the highly inhomogeneous Qdash system with a gradually uniform distribution of the carriers taking place at an elevated temperature that also assists in reducing the blueshift of F-P modes, due to the additional photon reabsorption and carrier spillover process that assists in this accomplishment. In general, high-energy photons (generated by small average height dashes with shallow conduction band offsets, i.e., exhibiting large transition energies) are absorbed by large average height dashes with deep conduction band offsets (small transition energies). Consequently, excitation of carriers to higher density states of the respective dash energy levels might be possible. Moreover, carriers from shallow conduction band offset dashes (i.e., small average height dashes) might escape via thermal excitation, tunneling, and thermally assisted tunneling processes and are trapped in other large average height dashes, thus allowing a relatively uniform distribution of carriers across the dispersive dashes in the active region. In fact, a broader lasing emission coverage is observed at elevated temperatures, very recently, from the chirped barrier thickness Qdash lasers,[19] thereby further supporting our attribution. Nevertheless, observation of near-constant $g_{\max}$ as well as the net modal gain slopes at different temperatures, and their appropriate alignment exhibiting an overall linear behavior between ~$0.75I_{\mathrm{th}}$ to $0.94I_{\mathrm{th}}$ indicates the consistency in the measured data.[10] In addition, the linear trend of F-P blueshift at all temperatures allows us to compare $\mathrm{d}g/\mathrm{d}I$, $\mathrm{d}n/\mathrm{d}I$, and hence α-factor at any of the common normalized bias conditions. To generalize our analysis further, we took the difference of the net modal gain and F-P mode shift between two bias currents at a fixed temperature and averaged over various measured current combinations (~$0.06I_{\mathrm{th}}$ average step). This facilitates comparing $\mathrm{d}g/\mathrm{d}I$, $\mathrm{d}n/\mathrm{d}I$, and α-factor values across 16°C to 35°C that are not only acceptable in their respective bias current range but also qualitatively be extended across ~$0.8I_{\mathrm{th}}$ to $0.94I_{\mathrm{th}}$ (~$0.88I_{\mathrm{th}}$ being the common bias) along with the variation margins. Furthermore, assuming that the slope of F-P mode shift at 40°C does not change appreciably at higher injections up to $\sim 0.88I_{\mathrm{th}}$, or more, we also compared the calculated results of $\mathrm{d}g/\mathrm{d}I$, $\mathrm{d}n/\mathrm{d}I$, and α-factor at this temperature with other temperatures in this work.

The spectral dependence of differential gain $\mathrm{d}g/\mathrm{d}I$ and differential refractive index change $\mathrm{d}n/\mathrm{d}I$ of the Qdash laser at various heatsink temperatures are calculated and plotted in Figs. 3(a) and 3(b), respectively. Considering Fig. 3(a), $\mathrm{d}g/\mathrm{d}I$ is found to be nearly uniform across ~ 1595 to 1620 nm for temperatures ≤25°C and extends to ~ 1625 nm for ≥30°C. This further supports our above discussion on an even rate of radiative recombination because of a uniform distribution of carrier concentration across the dispersive sizes dash ensembles in the active region encompassing at and around $g_{\max}$ (λ_g). Moreover, a decrease in $\mathrm{d}g/\mathrm{d}I$ is obvious at longer wavelengths at all operating temperatures. For temperatures ≤25°C, the rate of $\mathrm{d}g/\mathrm{d}I$ fall is sharp and onsets at ~ 1620 nm, whereas the rate slows down for ≥30°C and initiates at comparatively longer wavelengths, reaching ~ 1635 nm at 40°C. This is a consequence of the redshifting $g_{\max}$ with increasing temperature, which also shifts the small band transition energies of non-resonant large average height dashes to even smaller values as well. These large dashes exhibit a higher localized density of states and modal gain and hence require more carriers to overcome their localized losses first and then contribute to the overall gain of the active region. Hence, with an increase in carrier density, not much improvement in their gain is expected that imply degrading $\mathrm{d}g/\mathrm{d}I$ at longer wavelengths. Nonetheless, at $g_{\max}$, $\mathrm{d}g/\mathrm{d}I$ of $0.68 \pm 0.16\ \mathrm{cm}^{-1}\ \mathrm{mA}^{-1}$ is measured at 16°C, which diminishes slightly up to 25°C, but thereafter noticeably reaching a value of $0.23 \pm 0.1\ \mathrm{cm}^{-1}\ \mathrm{mA}^{-1}$ at 40°C. In general, this trend is consistent across all the spectra of $\mathrm{d}g/\mathrm{d}I$ at various temperatures and attributed qualitatively again to the extended inhomogeneous broadening of the Qdash system with increasing temperature. The uniform distribution of carriers across the highly dispersive Qdash energy states comes at an expense of escalated loss of the system via photon reabsorption and carrier spillover processes. Hence, a large operating current density at higher temperatures is required to extract gain from the active region, which leads to a lower overall differential gain. It is to be noted that the lasing peak wavelengths (not shown here) are found to detune to shorter wavelength relative to λ_g with increasing temperature at ~$0.88I_{\mathrm{th}}$. For instance, the lasing peak and λ_g are measured to be ~ 1610 and ~ 1615 nm at 16°C, respectively, whereas at 35°C, the lasing peak (~ 1618 nm) blueshifts by ~ 5 nm compared to λ_g (~ 1623 nm). Therefore, with a relatively flat $\mathrm{d}g/\mathrm{d}I$ spectrum around λ_g, within ~ 20 (~ 5) nm on the short (long) wavelength region, the values are expected to be alike around both peak gain and lasing peak wavelengths.

The wavelength dependence of $\mathrm{d}n/\mathrm{d}I$, which is plotted in Fig. 3(b), follows a similar trend in magnitude versus the laser diode operating temperature as observed for the case of $\mathrm{d}g/\mathrm{d}I$. While a minor decrease in value from $\sim(-2.2 \pm 0.25) \times 10^{-5}\ \mathrm{mA}^{-1}$ to $\sim(-2.1 \pm 0.25) \times 10^{-5}\ \mathrm{mA}^{-1}$

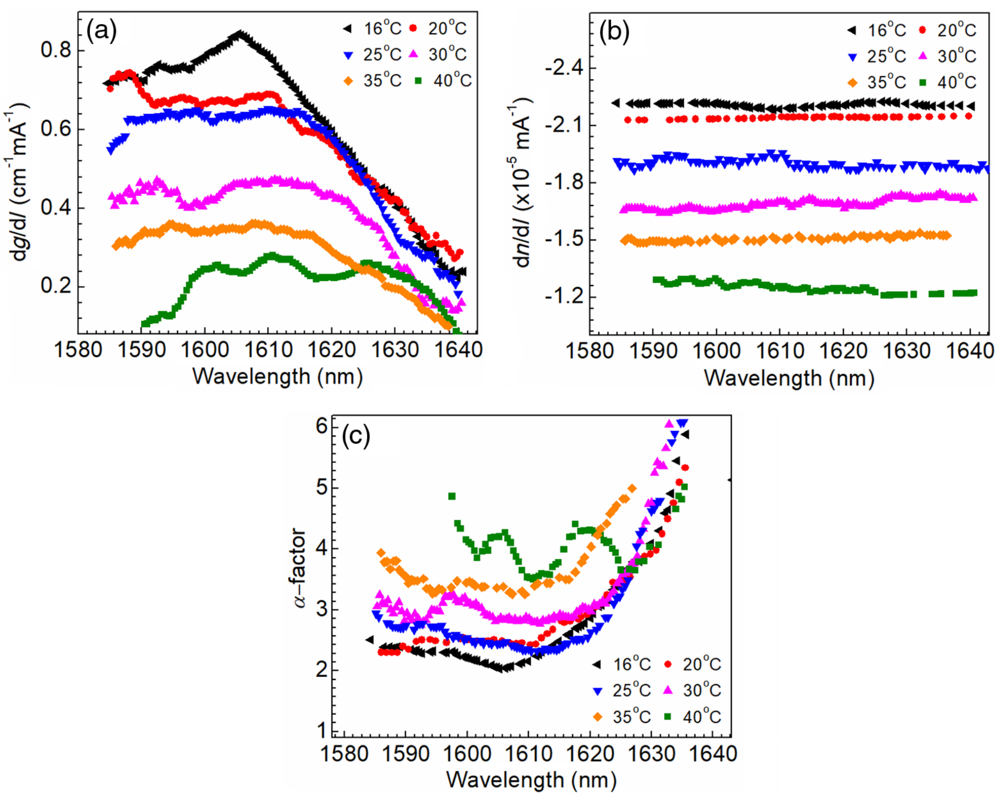

Fig. 3 (a) Differential modal gain ($\mathrm{d}g/\mathrm{d}I$), (b) differential refractive index change ($\mathrm{d}n/\mathrm{d}I$), and (c) α-factor of InAs/InP Qdash laser diode at various operating temperatures. Each temperature-dependent curve is an average of different combinations of two below threshold currents of Fig. 2(b), hence the curves qualitatively represent the characteristics across $\sim 0.8I_{th}$ to $0.94I_{th}$ with $\sim 0.88I_{th}$ being the common bias. The variation margins for $\mathrm{d}g/\mathrm{d}I$ are ± 0.16, ± 0.10, ± 0.10, ± 0.08, ± 0.14, and ± 0.1; $\mathrm{d}n/\mathrm{d}I$ are $\pm 0.28 \times 10^{-5}$, $\pm 0.25 \times 10^{-5}$, $\pm 0.45 \times 10^{-5}$, $\pm 0.72 \times 10^{-5}$, $\pm 0.50 \times 10^{-5}$, and $\pm 0.17 \times 10^{-5}$; and α-factor are ± 1.0, ± 1.0, ± 1.0, ± 1.5, ± 1.5, ± 2.0, corresponding to 16°C, 20°C, 25°C, 30°C, 35°C, and 40°C, respectively.

is measured up to 25°C at $g_{\max}$, the magnitude thereafter drops appreciably with rising temperature, reaching $\sim(-1.5 \pm 0.5) \times 10^{-5}\ \mathrm{mA}^{-1}$ and $\sim(-1.2 \pm 0.17) \times 10^{-5}\ \mathrm{mA}^{-1}$ at 35°C and 40°C, respectively. As discussed above, this observation is attributed in part to the inverse relation of carrier density with the medium refractive index and in part to the uniform distribution of carriers among the density states of the highly dispersive and closely spaced Qdash energy levels with increasing temperature. The evenly dispersed localized carrier concentration results in relatively symmetric gain spectra and tends to reduce the active region refractive index at elevated temperatures, thus leading to smaller magnitudes of $\mathrm{d}n/\mathrm{d}I$, and further supported by Kramers–Kronig relation.[20] This is also reflected by the decreasing rate of F-P blueshift with bias with increasing temperature, as shown in Fig. 2(c). Also, note that a relatively flat profile around λ_g is observed in Fig. 3(b) with a small decrease in the magnitude of $\mathrm{d}n/\mathrm{d}I$ by $\sim(1.0 \pm 0.3) \times 10^{-5}\ \mathrm{mA}^{-1}$ noticed between 16°C and 40°C. Hence, in the subsequent analysis, we concentrated our discussion at λ_g since similar value of $\mathrm{d}g/\mathrm{d}I$ and $\mathrm{d}n/\mathrm{d}I$ would be exhibited at the lasing peak wavelengths.

Figure 3(c) shows the resulting spectral evolution of the α-factor of the InAs/AlGaInAs/InP Qdash laser as a function of operating temperature, obtained from the derivatives in Figs. 3(a) and 3(b). In general, at a constant temperature, the spectrum resembles that of quantum-wire-like dependence indicated by an increase (rapid rise) in α-factor at shorter (longer) wavelengths, followed by the presence of a minimum value in between.[12] Moreover, it can be inferred that the α-factor value escalates with the rise in temperature while remaining relatively flat near $g_{\max}$ and the lasing peak wavelengths, due to the near flat profiles of $\mathrm{d}g/\mathrm{d}I$ and $\mathrm{d}n/\mathrm{d}I$ across the spectral range. At 16°C heatsink temperature, despite of the large magnitude of $\mathrm{d}n/\mathrm{d}I$, the resulting α-factor is found to be within $\sim$(2.0 to 2.5)$\pm$1.0 in the wavelength range $\leq$1620 nm, and slightly increases to $\sim$(2.3 to 3.0)$\pm$1.0 at 25°C. Furthermore, the value rises to $\sim$(3.3 to 4.3)$\pm$1.5 at 35°C and $\sim$(3.5 to 4.7)$\pm$2.0 at 40°C within an extended wavelength range of $\sim$1600 to 1625 nm and $\sim$1600 to 1635 nm (which includes the respective λ_g and lasing peak), respectively, regardless of exhibiting reduction in magnitude of $\mathrm{d}n/\mathrm{d}I$ with rise in temperature. Hence, from this observation, we deduce a stronger influence of $\mathrm{d}g/\mathrm{d}I$ compared to $\mathrm{d}n/\mathrm{d}I$ in deciding the α-factor since the former decreased by a factor of $\sim$3.0 and the latter dropped by a mere factor of $\sim$1.7, on increasing the temperature from 16°C to 40°C. Hence, the temperature-dependent gain dynamics in the inhomogeneous Qdash system plays a major role for large α-factor values at elevated temperatures.

Lastly, we show the influence of heatsink temperature on $\mathrm{d}g/\mathrm{d}I$, $\mathrm{d}n/\mathrm{d}I$, and α-factor of the Qdash laser at $g_{\max}$ in Fig. 4(a) alongside the variation margin that includes the disparity of values across various below threshold current combinations as well as across different laser devices tested. A clear dual-trend regime is noticeable in all the three curves of Fig. 4(a), with a device temperature of 25°C being the boundary between the regions. The data markers are then fitted in each region assuming a linear relationship to identify the rate of change in $\mathrm{d}g/\mathrm{d}I$, $\mathrm{d}n/\mathrm{d}I$, and α-factor with temperature. A reasonable linear fitting in both the regions across all the three curves is accomplished. In view of low-temperature regime ($\leq$25°C), $\mathrm{d}g/\mathrm{d}I$ decreases at a meager rate of $\sim$0.001 cm^{-1} mA^{-1} C^{-1} whereas the magnitude of $\mathrm{d}n/\mathrm{d}I$ slope dropped at a rate of $\sim -4.6\times10^{-7}$ mA^{-1}°C^{-1} thereby resulting in a negligible change ($\sim$0.01°C^{-1}) of α-factor in this region, sustaining a value of $\sim 2.6 \pm 1.0$. This extracted α-factor is slightly large, yet, in good agreement with the reported values of $\sim$2.0 in the literature for fixed barrier thickness InAs/InP Qdash lasers around $\sim$1610 nm.[10] It is noteworthy to mention here that being a chirped barrier thickness device with an extended active region inhomogeneity, the measured α-factor degraded by a small ratio of $\sim$1.3 compared to fixed barrier thickness Qdash laser. In addition, this factor is better than the experimentally and numerically reported ratios of $\sim$5.5 (α-factor of $\sim$0.313 from chirped compared to $\sim$0.057 from unchirped device) and $\sim$1.1 for InAs/GaAs quantum-dot lasers devices.[21,22] This obtained value of α-factor implies that mixed

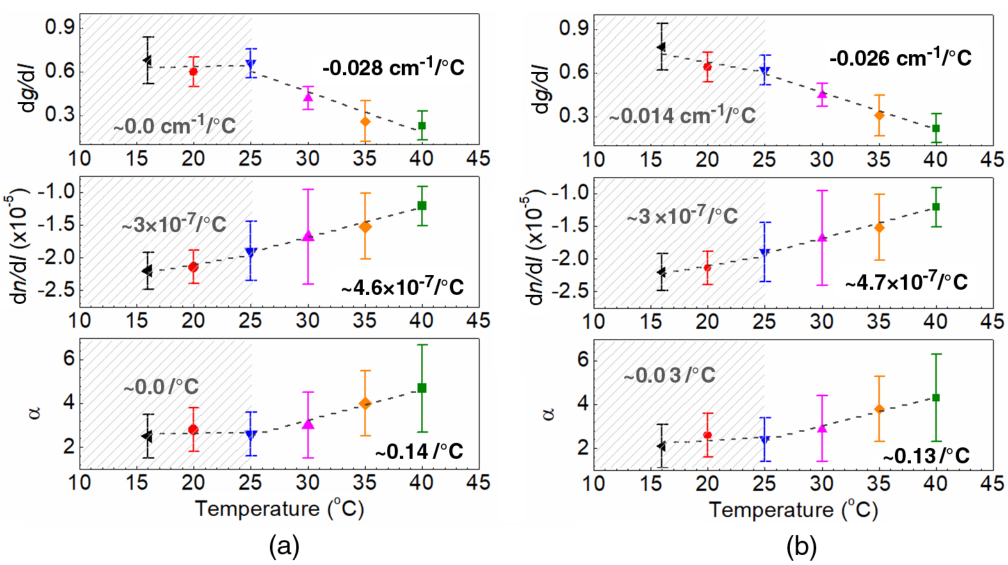

Fig. 4 $\mathrm{d}g/\mathrm{d}I$ (top), $\mathrm{d}n/\mathrm{d}I$ (center), and α-factor (bottom) of InAs/InP Qdash laser diode versus the operating temperature, obtained from Fig. 3 at (a) $\sim 0.88I_{\mathrm{th}}$ gain maximum and (b) threshold lasing peak, along with the variation margin of Fig. 3. The dash lines are the linear fitting in the two regions, low (shaded) and high (unshaded) temperature with 25°C as the boundary. The measured λ_g (lasing peak) at $\sim 0.88I_{\mathrm{th}}$ ($1.01I_{\mathrm{th}}$) are $\sim$1615 ($\sim$1610), $\sim$1617 ($\sim$1613), $\sim$1619 ($\sim$1614), $\sim$1620 ($\sim$1615), $\sim$1623 ($\sim$1618), and $\sim$1630 ($\sim$1620) nm, corresponding to 16°C, 20°C, 25°C, 30°C, 35°C, and 40°C, respectively. The numbers in each temperature region of the figure are the obtained respective slope values from the linear fitting. The variation margins follows that of Fig. 3.

dot-like and wire-like features of Qdash with the overlapping density of states with high-energy tail favor improved dynamic laser characteristics compared to inhomogeneous Qwell or quantum-dot active region lasers. On the other front, in the high-temperature region (≥25°C), a considerable degradation in the dynamic characteristics of the laser is noted. While a steady decrease of $\mathrm{d}g/\mathrm{d}I$ is noticed compared to the low-temperature region, exhibiting a value of $\sim 0.03\ \mathrm{cm}^{-1}\ \mathrm{mA}^{-1}{}^{\circ}\mathrm{C}^{-1}$, the magnitude of $\mathrm{d}n/\mathrm{d}I$ also showed a higher rate of fall $\sim 3.0 \times 10^{-7}\ \mathrm{mA}^{-1}{}^{\circ}\mathrm{C}^{-1}$. The resultant rate of rise in α-factor due to this combined effect is calculated to be $\sim 0.14{}^{\circ}\mathrm{C}^{-1}$ that is again an increase by a factor of ~14 compared to the low-temperature region, thus further supporting our attribution of $\mathrm{d}g/\mathrm{d}I$ as the dominating term in determining the α-factor of the device at different operating temperatures. In Fig. 4(b), we plot $\mathrm{d}g/\mathrm{d}I$, $\mathrm{d}n/\mathrm{d}I$, and α-factor of the Qdash laser at the peak lasing wavelength. A slight decrease in the rate of $\mathrm{d}g/\mathrm{d}I$, in this case, reaching a value of $\sim 0.014\ \mathrm{cm}^{-1}\ \mathrm{mA}^{-1}{}^{\circ}\mathrm{C}^{-1}$ in the low-temperature region, and an analogous $\mathrm{d}n/\mathrm{d}I$ compared to Fig. 4(a), caused a slight rise of α-factor in this temperature region reaching a value of $\sim 0.03{}^{\circ}\mathrm{C}^{-1}$. However, for the high-temperature regime, the dynamic characteristics obtained at the lasing peak are similar to λ_g, an effect of relatively flat $\mathrm{d}g/\mathrm{d}I$ and $\mathrm{d}n/\mathrm{d}I$ around these wavelengths due to a broad gain profile of the Qdash active region with extended inhomogeneous broadening. This comprehensive analysis of $\mathrm{d}g/\mathrm{d}I$, $\mathrm{d}n/\mathrm{d}I$, and α-factor shows a strong influence of operating temperature on the frequency chirp performance of InAs/InP Qdash lasers and our qualitative analysis with brief physical insight into the device active region may provide a guideline for future design and optimization of these laser devices for high bit-rate communication applications.

4 Conclusion

Below threshold gain and α-factor of L-band chirped barrier thickness InAs/InP Qdash laser diode at various operating temperatures were measured with H-P method. The obtained results at peak gain showed two operating regimes with an insensitive low-temperature region up to 25°C where nearly constant dynamic characteristics were observed, with α-factor exhibiting a nearly flat value of $\sim 2.6 \pm 1.0$ within ~1590 to 1625 nm. However, the performance degraded in the high-temperature region (≥25°C) with a considerable reduction in the differential gain and a resultant drop of α-factor at a rate of $\sim 0.14{}^{\circ}\mathrm{C}^{-1}$ and exhibiting values of $\sim 3.8 \pm 1.5$ at 35°C and $\sim 4.7 \pm 2.0$ at 40°C, at the gain maximum. The α-factor decreased slightly at 20°C but still is relatively comparable to the less inhomogeneous fixed barrier thickness InAs/InP Qdash laser. Our work essentially identifies the limitations of chirped barrier thickness broadband Qdash laser diodes at ~1610 nm in high-temperature applications and provides possible directions toward improvement for temperature-sensitive applications, such as, optical sources in extended L-band next-generation optical access network that is under consideration.

Acknowledgments

The author thanks King Fahd University of Petroleum and Minerals (KFUPM) and acknowledges the support of King Abdulaziz City for Science and Technology (KACST) through KACST Technology Innovation Center (TIC) on Solid State Lighting (SSL) "KACST-TIC on SSL" under Grant No. KACST TIC R2-FP-008 and EE2381.

References

1. J. P. Reithmaier, G. Eisenstein, and A. Forchel, "InAs/InP quantum-dash lasers and amplifiers," *Proc. IEEE* **95**(9), 1779–1790 (2007).
2. M. T. A. Khan et al., "100 Gb/s single channel transmission using injection-locked 1621 nm quantum-dash laser for WDM-based optical access network," *IEEE Photonics Technol. Lett.* **29**(6), 543–546 (2017).
3. M. A. Shemis et al., "Broadly tunable self-injection locked InAs/InP quantum-dash laser based fiber/FSO/hybrid fiber-FSO communication at 1610 nm," *IEEE Photonics J.* **10**(2), 1–10 (2018).

4. B. S. Ooi et al., “Quantum dashes on InP substrate for broadband emitter applications,” *IEEE J. Sel. Top. Quantum Electron.* **14**(4), 1230–1238 (2008).
5. V. Vujicic et al., “Quantum dash mode-locked lasers for data centre applications,” *IEEE J. Sel. Top. Quantum Electron.* **21**(6), 53–60 (2015).
6. R. Rosales et al., “High performance mode locking characteristics of single section quantum dash lasers,” *Opt. Express* **20**(8), 8649–8657 (2012).
7. J. P. Tourrenc et al., “Experimental investigation of the timing jitter in self-pulsating quantum-dash lasers operating at 1.55 μm,” *Opt. Express* **16**(22), 17706–17713 (2008).
8. A. J. Zilkie et al., “Carrier dynamics of quantum-dot, quantum-dash, and quantum-well semiconductor optical amplifiers operating at 1.55 μm,” *IEEE J. Quantum Electron.* **43**(11), 982–991 (2007).
9. C. Wang et al., “Thermally insensitive determination of the linewidth broadening factor in nanostructured semiconductor lasers using optical injection locking,” *Sci. Rep.* **6**, 27825 (2016).
10. C. Chen et al., “Effects of intermixing on gain and alpha factors of quantum-dash lasers,” *IEEE Photonics Technol. Lett.* **20**(19), 1654–1656 (2008).
11. S. Hein, S. Hofling, and A. Forchel, “Modulation bandwidth and linewidth enhancement factor of high-speed 1.55 μm quantum-dash lasers,” *IEEE Photonics Technol. Lett.* **21**(8), 528–530 (2009).
12. A. A. Ukhanov et al., “Orientation dependence of the optical properties in InAs quantum-dash lasers on InP,” *Appl. Phys. Lett.* **81**(6), 981–983 (2002).
13. Z. Mi and P. Bhattacharya, “DC and dynamic characteristics of P-doped and tunnel injection 1.65 μm InAs quantum-dash lasers grown on InP (001),” *IEEE J. Quantum Electron.* **42**(12), 1224–1232 (2006).
14. F. Lelarge et al., “Recent advances on InAs/InP quantum dash based semiconductor lasers and optical amplifiers operating at 1.55 μm,” *IEEE J. Sel. Top. Quantum Electron.* **13**(1), 111–124 (2007).
15. L. F. Lester et al., “Strong optical injection and the differential gain in a quantum dash laser,” *Opt. Express* **22**(6), 7222–7228 (2014).
16. Z. J. Jiao et al., “Linewidth enhancement factor of InAs/InP quantum dot lasers around 1.5 μm,” *Opt. Commun.* **285**, 4372–4375 (2012).
17. S. Bhowmick et al., “High performance $InAs/In_{0.53}Ga_{0.23}Al_{0.24}As/InP$ quantum dot 1.55 μm tunnel injection laser,” *IEEE J. Quantum Electron.* **50**(1), 7–14 (2014).
18. M. A. Shemis et al., “Demonstration of L-band DP-QPSK transmission over FSO and fiber channels employing InAs/InP quantum-dash laser source,” *Opt. Commun.* **410**, 680–684 (2018).
19. E. Alkhazraji et al., “Effect of temperature and ridge-width on the lasing characteristics of InAs/InP quantum-dash lasers: a thermal analysis view,” *Opt. Laser Technol.* **98**, 67–74 (2018).
20. Z. Xu et al., “Submonolayer InGaAs/GaAs quantum-dot lasers with high modal gain and zero-linewidth enhancement factor,” *Appl. Phys. Lett.* **85**(15), 3259–3261 (2004).
21. K. C. Kim et al., “Gain-dependent linewidth enhancement factor in the quantum dot structures,” *Nanotechnology* **21**(13), 134010 (2010).
22. C. L. Tan et al., “The dynamic characteristics and linewidth enhancement factor of quasi-supercontinuum self-assembled quantum dot lasers,” *IEEE J. Quantum Electron.* **45**(9), 1177–1182 (2009).

Mohammed Zahed Mustafa Khan received a PhD in electrical engineering from King Abdullah University of Science and Technology (KAUST), Saudi Arabia, in 2013, and later was a postdoctoral fellow at KAUST for a year. Since 2015, he has been an assistant professor in the Electrical Engineering Department, King Fahd University of Petroleum and Minerals, Saudi Arabia. His research focus is on the development and applications of visible and near-infrared semiconductor lasers in optical communications.